Available online at www.sciencedirect.com
SCIENCE DIRECT®
International Journal of Heat and Fluid Flow 26 (2005) 495–505
International Journal of HEAT AND FLUID FLOW
www.elsevier.com/locate/ijhff

A model of the capillary limit of a micro heat pipe and prediction of the dry-out length

Balram Suman, Sirshendu De, Sunando DasGupta *

Department of Chemical Engineering, Indian Institute of Technology, Kharagpur 721302, India

Received 15 April 2004; accepted 16 September 2004
Available online 21 November 2004

Abstract

A model for fluid flow and heat transfer in a micro heat pipe of any arbitrary (polygonal) shape is presented utilizing a macroscopic approach. The coupled non-linear governing equations for the fluid flow, heat and mass transfer are developed based on first principles and are solved numerically. The performance and the capillary limitations of such a device are analyzed in detail. The profile of the radius of curvature is used to predict the onset of the dry-out point and the propagation of the dry out length. A method is developed to estimate the dry out length as a function of system geometry and process variables, e.g., heat input and inclination. The model predicted results are successfully compared with the experimental results from a previous study. The general nature of the model and the associated parametric study ensure the wide applicability of the model.

Keywords: Micro heat pipes; Capillary forces; Critical heat input; Dry-out length; Modeling

1. Introduction

Micro scale heat exchange is currently an active area of research due to its possible applications in several technologically important processes requiring augmented heat transfer e.g., in the electronic packaging industry, in micro gravity environments, and space craft thermal control. Although the use of micro heat pipes for enhanced heat transfer are becoming increasingly common, the exact nature of liquid evaporation from the corners of a micro heat pipe and the associated capillary pumping capacity need to be investigated in detail. The generalized treatment of fluid flow and capillary limitation of a system of micro heat pipe of any geometry and inclination is relevant for the complete understanding of the transport processes and the design of such devices.

Cotter (1984) first proposed the concept of micro heat pipe, which essentially is a wickless heat pipe for the uniform temperature distribution in electronic chips. In practical terms, a micro heat pipe is a wickless, non-circular channel with a diameter of 10–500 μm and a length of 10–20 mm. The flow of fluids inside the pipe is caused by the change in pressure (due to changes in capillary and intermolecular force field) along the length of the heat pipe. The net capillary force is generated by the integral effect of the evaporating and condensing menisci (Swanson and Herdt, 1992). The surface tension forces, wettability and the solid–liquid interactions primarily govern the behavior of the various interfaces, particularly the liquid–vapor interface (Derjaguin and Chyraev, 1976; Troung and Wayner, 1987; Moosman and Homsy, 1980; Gee et al., 1989; Bankoff, 1990; Anderson and Davis, 1995; DasGupta et al., 1995). The existing models (Wayner et al., 1976; Renk and Wayner, 1979; Wayner, 1991) of stable evaporating meniscus are based on the hypothesis that the fluid flow in the evaporating meniscus results from a change in the meniscus profile

* Corresponding author. Tel.: +91 3222 283922; fax: +91 3222 255303.
E-mail address: sunando@che.iitkgp.ernet.in (S. DasGupta).

0142-727X/$ - see front matter © 2004 Published by Elsevier Inc.
doi:10.1016/j.ijheatfluidflow.2004.09.006

Nomenclature

a	side length of a regular polygon or smaller side of a rectangle, m
a_1	larger side length of a rectangle, m
A_{cs}	area of cross-section of substrate available for conduction of heat, m^2
A_l	total liquid area, m^2
A'_l	liquid area of one corner, m^2
B_1	constant in expression for A_l
B_2	constant in expression for $\frac{dR^*}{dX^*}$ [Eq. (5)]
ch	channel
D_h	hydraulic diameter, m
f	friction factor
g	acceleration due to gravity, m/s^2
K'	constant in expression for B_2
K_s	thermal conductivity of substrate, W/mK
L	length of heat pipe, m
L_h	half of total wetted length, m
L'_h	half of wetted length for one corner, m
n	number of sides of a polygon
N_{Re}	Reynolds number
P	liquid pressure, N/m^2
P^*	non-dimensional liquid pressure
P_R	reference pressure, N/m^2
P_{v_0}	pressure in vapor region, N/m^2
Q	net heat flux supplied to the liquid, W/m^2
Q'	net heat supplied, W
Q_v	heat flux for vaporization of liquid, W/m^2
R	radius of curvature, m
R^*	non-dimensional radius of curvature
R_0	reference radius, m
Re	rectangle
R_l	meniscus surface area per unit length, m
T	temperature of substrate, °C
Tr	triangle
V	axial liquid velocity, m/s
$\|V\|$	magnitude of axial liquid velocity, m/s
V^*	non-dimensional liquid velocity
V_R	reference liquid velocity, m/s
W_b	polygon pitch, m
x	coordinate along the heat pipe, m
X^*	non-dimensional coordinate along heat pipe
Greeks	
α	half apex angle of polygon, radian
β	inclination of substrate with horizontal, radian
γ	contact angle, radian
ϕ	curvature, m^{-1}
λ	latent heat of vaporization of coolant liquid, J/kg
μ	viscosity of coolant liquid, kg/ms
ρ	density of coolant liquid, kg/m^3
σ	surface tension of coolant liquid, N/m
τ_w	wall shear stress, N/m^2

(DasGupta et al., 1993a,b), which creates the necessary pressure gradient and demonstrate the importance of the various regions of a thin film during evaporative heat transfer (Zheng et al., 2004) as well as condensation and spreading (Gokhale et al., 2004).

Important contributions to the related area of heat transfer from small devices were made by Peterson and his co-workers. Babin et al. (1990) tested a trapezoidal heat pipe with a square cross-section of $1\,mm^2$ and a length of 57 mm. Wu and Peterson (1991) studied a wickless micro heat pipe of dimension $1 \times 1 \times 10$–$100\,mm^3$. They successfully used the Young–Laplace equation to describe the internal fluid dynamics of this integrated device. The interfacial thermodynamics of micro heat pipes was studied by Swanson and Peterson (1995). From these works, it has been concluded that the longitudinal groove design is crucial to increase the heat transport capacity of these miniature devices and the smaller grooves provide the necessary capillary forces for the liquid to flow back into the evaporative zone. The minimum meniscus radius and maximum heat transport in triangular grooves have been also studied (Peterson and Ma, 1996). Khrustalev and Faghri (1995) developed a mathematical model to describe heat transfer through thin liquid films in the evaporator region of heat pipes with capillary grooves. Detailed thermal analysis and evaluation of different limitations of micro heat pipes were performed by Khrustalev and Faghri (1994). Xu and Carey (1990) developed an analytical model for evaporation from a V-shaped micro grooved surface assuming that the evaporation takes place only from the thin film region of the meniscus. Stephan and Busse (1992) have presented a model for the calculation of the radial heat transfer coefficient in heat pipes with open grooves and have shown that the assumption of an interface temperature equal to the saturation temperature of the vapor leads to a large over-prediction of the radial heat transfer coefficient. Ravikumar and DasGupta (1997) presented an integrated model of evaporation from V-shaped micro grooves. Their model incorporates the evaporation from the capillary as well as the transition region of the extended meniscus as a function of groove length. In recent years, many researchers have investigated the concept of using micro heat pipes as effective heat spreaders (Ma and Peterson, 1996; Khan et al., 1999).

In the work of Ha and Peterson (1998), an analytical solution is presented using a quadratic profile of the evaporative heat flux for small tilt angles. This work provides useful information on the design restrictions and utility of micro heat pipes. Anand et al. (2002) extended the theoretical model of Ha and Peterson (1998) and controlled experiments were performed to pinpoint the onset of the dry-out and its propagation along the length of the heat pipe, as a function of system parameters, for large tilt angles. The experimentally obtained temperature profiles were analyzed to evaluate the evaporative heat flux as a function of position, which was used in the numerical solution of the model. The prediction of the occurrence and position of the dry-out point was successfully compared with the experimental observations. Catton and Stroes (2002) presented a one-dimensional, semi analytical model for prediction of the wetted length supported by inclined triangular capillary grooves. The concept of accommodation theory was introduced to account for the change in radius of curvature of the liquid–vapor interface.

In the present work, a macroscopic approach is used to develop a general model for a heat pipe with grooves of any shape. The axial flow of the liquid is modeled as a result of the change in the radius of curvature. The effect of body forces is also taken into account. The coupled non-linear governing equations for the fluid flow, heat and mass transfer are solved numerically. The profile of the radius of curvature is used to predict the onset of the dry-out point. A method is developed to estimate the dry out length as a function of system geometry and process variables, e.g., heat input, inclination etc. The model predictions are successfully compared with the experimental data of dry-out length from a previous study (Anand et al., 2002).

2. Theory

The system being studied herein consists of axially grooved micro heat pipe with grooves of any polygonal shape. Though the model equations are general in nature in terms of the shape of the grooves, an equilateral triangular and a rectangular heat pipe have been studied herein as test cases. The heat pipe is inclined at an angle to provide a body force. Due to capillary pumping, the liquid will be pushed towards the hot end. The liquid will travel along the corners and the vapor passes through the open space (Fig. 1). The hot and the cold ends denote the farthest end of evaporative and the condenser region, respectively. The heat flux distribution in the evaporative and condenser regions is considered to be of constant value.

The capillary pumping and associated flow of the liquid towards the hot end is a result of the decrease in the radius of curvature caused by the intrinsic meniscus

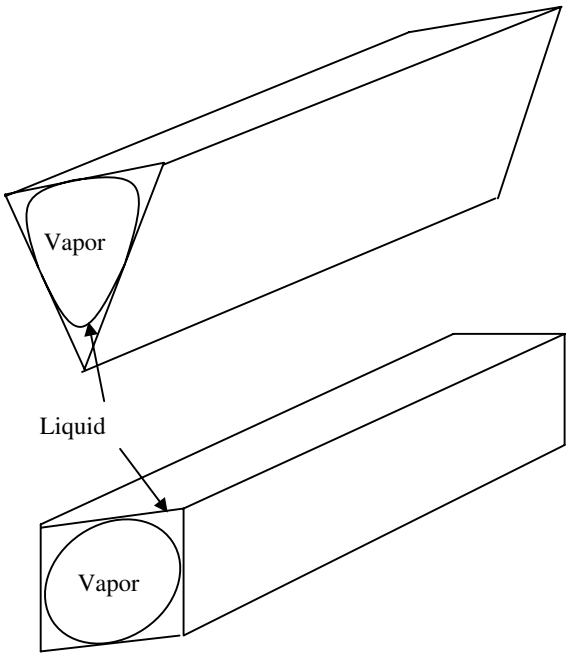

Fig. 1. Schematic of the triangular and rectangular heat pipes.

receding into the corner. The change in the radius of curvature results in an associated decrease in the liquid pressure forming the driving force for such a flow. As the liquid recedes further towards the apex of the corner, the liquid film gradually becomes thinner and more curved (lower radius of curvature). The radius of curvature at the cold end is a constant ($R = R_0$) calculated from the geometry of the groove.

It is shown earlier (Peterson and Ma, 1996; Ha and Peterson, 1998) that the capillary forces primarily cause the axial flows. The capillary forces are directly proportional to the product of surface tension of liquid and inverse of the radius of curvature. The radius of curvature of the liquid film is a function of the axial position. The model presented herein develops the governing equations for fluid flow, heat transfer and relate them to capillary forces present in the system. The model equations are developed for all three regions, i.e., evaporative, adiabatic, and condenser encompassing the complete heat pipe.

The governing model equations are derived under the following assumptions: (i) one dimensional steady incompressible flow along the length of heat pipe; (ii) uniform distribution of heat input; (iii) negligible viscous dissipation; (iv) constant pressure in the vapor region in the operating range of temperature; (v) one dimensional temperature variation along the length of heat pipe; (vi) shear stress at the liquid vapor interface has been neglected.

The radius of curvature at the cold end (R_0) can be calculated from geometry as presented in Appendix A. It is established later that the body force is small compared to the force due to pressure jump at the vapor

liquid interface and thus the meniscus at each corner is independent of orientation. The evaluation of relevant geometrical parameters, depending on number of corners, is presented in Appendix A. One corner of a section of a heat pipe of any polygonal shape of length Δx is shown in Fig. 2. The radius of curvature, liquid velocity and pressure vary along the length of pipe. The wall shear stress, τ_w, acts against the liquid flow. The liquid pressure as a function of the radius of curvature can be estimated from the Young–Laplace equation in differential form,

$$\frac{dP}{dx} = \frac{\sigma}{R^2}\frac{dR}{dx} \tag{1}$$

The terms $\frac{dP}{dx}$ and $\frac{dR}{dx}$ are the pressure gradient and radius of curvature gradient, respectively. The steady state momentum balance in differential form is

$$\rho A_l V \frac{dV}{dx} + A_l \frac{dP}{dx} + 2L_h\tau_w - \rho g \sin(\beta) A_l = 0 \tag{2}$$

The first term in the above equation represents the convective momentum change, the second term is the pressure force acting on the volume element, the third term represents the wall shear force and the fourth term is gravity force.

At steady state, the difference between the mass entering and leaving the volume element is equal to the mass evaporated from that volume element. Thus the differential form of the mass balance is

$$\frac{d}{dx}(\rho V A_l) + \frac{Q_v R_l}{\lambda} = 0 \tag{3}$$

The first term in Eq. (3) represents the change of the liquid mass due to convection and the second term represents the mass of the liquid evaporated. R_l represents the meniscus surface area per unit length of the heat pipe.

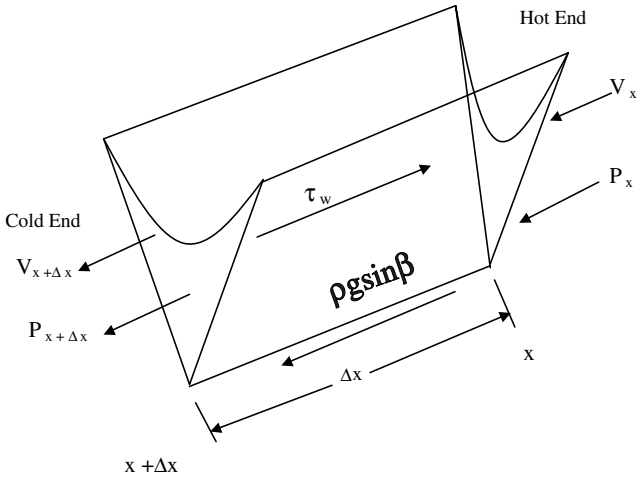

Fig. 2. Volume element of the one corner of the polygon with all forces specified.

Both the terms in the above equation are functions of radius of curvature (R) and vary along with the length of the heat pipe. The total meniscus surface area can be obtained by integrating $R_l dx$ along the length of the heat pipe.

A part of the supplied heat is used to raise the temperature of the liquid packet while the remaining heat is used for evaporation. It was shown by Ravikumar and DasGupta (1997) that the sensible heat content is very small compared to the heat used for the evaporation and condensation. Hence, the sensible heat content can safely be neglected. Thus, the energy balance in the volume element can be expressed as

$$QW_b - Q_v R_l = 0 \tag{4}$$

where Q is the input heat flux taken up by the coolant liquid from the substrate. Q is positive in the evaporative section and negative in the condenser section. The first term in Eq. (4) represents the heat supplied to the element and the second term represents the heat leaving the element due to evaporation.

2.1. Boundary conditions

The liquid velocity is zero at $x = 0$ since there is no evaporation beyond the hot end ($x = 0$). The radius of curvature of the liquid meniscus at the cold end ($x = L$), R_0 is a constant and can be obtained from geometry for filled groove with a liquid with a known contact angle system. The coupled ODEs (1)–(3) are solved with the help of Eq. (4) and boundary conditions:

$$\text{at} \quad x = 0, \quad V = 0$$
$$\text{at} \quad x = L, \quad R = R_0 \quad \text{and} \quad P = P_{v_0} - \tfrac{\sigma}{R_0}$$

2.2. Non-dimensionalization

Eqs. (1)–(3) are non-dimensionalized using the following expressions: friction factor, $f = K'/N_{Re}$, hydraulic diameter, $D_h = 4A_l/(2L_h)$, Reynolds number, $N_{Re} = D_h\rho V/\mu$, wall shear stress, $\tau_w = \rho V^2 f/2$, reference velocity, $V_R = Q'/(\rho R_0^2 \lambda)$, reference pressure, $P_R = \sigma/R_0$. The dimensionless parameters are defined as follows: R^* (dimensionless radius of curvature) $= R/R_0$; X^* (dimensionless position) $= x/L$; V^* (dimensionless liquid velocity) $= V/V_R$; P^* (dimensionless liquid pressure) $= P/P_R$. K' is used in the expression of the friction factor, f, and is a constant for a specific geometry (13.33 for triangle and 15.55 for rectangle with side ratio 1:2, (Ayyaswamy et al., 1974)). R_0 is the radius of curvature at the cold end and is a function of side length, contact angle for the substrate and coolant liquid combination and the apex angle of the polygon. After non-dimensionalization and rearrangement, Eqs. (1)–(3) result into the following equations:

$$\frac{dR^*}{dX^*} = \frac{\left[\rho g \sin(\beta) + \frac{Q_v V_R R_l V^*}{A_l \lambda} - \frac{B_2 V_R V^*}{(R_0 R^*)^2}\right]}{\left[\frac{\sigma}{R_0 L R^{*2}} - 2\rho \frac{V_R^2 V^{*2}}{L R^*}\right]} \quad (5)$$

$$\frac{dV^*}{dX^*} = -\left[\frac{Q_v R_l L}{\rho A_l \lambda V_R} + 2\frac{V^*}{R^*}\frac{dR^*}{dX^*}\right] \quad (6)$$

$$\frac{dP^*}{dX^*} = \frac{\sigma}{R_0 P_R R^{*2}}\frac{dR^*}{dX^*} \quad (7)$$

For a known input heat flux, the heat flux distribution at the meniscus surface can be evaluated from Eq. (4) as

$$Q_v = \frac{QW_b}{R_l} \quad (8)$$

where A_l, W_b, R_l, B_2 and B_1 are defined in Appendix A.

The dimensionless boundary conditions are as follows:

at $X^* = 0$ $V^* = 0$

at $X^* = 1.0$ $R^* = 1.0$

and $P^* = \left[P_{v_0} - \sigma/(R^* R_0)\right]/P_R$ at any X^*

Eqs. (5)–(8) are valid for all the three regions of the heat pipe namely, evaporative, adiabatic and condenser. In Eq. (8), Q is positive, zero and negative for the evaporative, adiabatic and condenser regions, respectively.

2.3. Numerical solution

The coupled model equations are solved using an iterative procedure. Runga-Kutta fourth-order integration routines are used. The inputs are heat distribution for the evaporative and the condenser regions, geometry of the heat pipe, contact angle for the substrate and coolant liquid combination and thermophysical properties of the coolant liquid. The initial value of R^* at the hot end ($X^* = 0.0$) is assumed and the equations are integrated from $X^* = 0$ to $X^* = 1.0$. R^* should be equal to 1.0 at the cold end ($X^* = 1.0$). If the obtained value of R^* at the cold end is not equal to 1.0, a new value of R^* at the hot end is assumed and the integration process is repeated till the conditions $R^* = 1.0$ within a tolerance limit at $X^* = 1.0$ is achieved. The integration step sizes are progressively reduced from 1.0×10^{-2} till the values of the dependent variables evaluated become independent of the step size. The step size chosen in this study is 1.0×10^{-4}.

3. Results and discussion

Two test cases are analyzed and the model is validated with results available in the literature (Anand et al., 2002). The heat pipes selected for this study are (i) an equilateral triangular heat pipe with each side equal to 400 μm and (ii) a rectangular (800 μm × 400 μm) heat pipe. The model is also valid for any regular polygon with number of sides greater than four. Both the heat pipes are of 2 cm length. The lengths for the evaporative, the adiabatic and the condenser regions are assumed to be equal. For the parametric study, the temperature difference between the hot and the cold end is taken to be equal to 5 °C and the angle of inclination is 10°. The cold end temperature is taken to be 32 °C. The temperature at the cold end and the temperature difference ($\Delta T = 5$ °C) between the hot and the cold end have been specified to calculate the thermophysical properties of coolant liquid. Thus the properties have been calculated at the average temperature of the hot and the cold end i.e., at 34.5 °C. Constant heat distribution is taken in the evaporator and the condenser section. Pentane is the working fluid with silicon as the substrate. Pentane wets silicon completely, i.e., γ (contact angle) is zero. The system studied in this work is a perfectly wetting system ($\gamma = 0$). If it is partially wetting, that may have some effect on the radius of curvature and hence the available liquid area. However for small contact angles this effect may not be substantial. A detailed study of the effect of contact angle is beyond the scope of the present work. The origin of the coordinate system used herein is at the hot end ($X^* = 0$). In the subsequent figures, Tr and Re are used to denote triangular and rectangular heat pipes, respectively and the numerals 1, 2 are used to denote different operating conditions in terms of the varying heat input.

The radius of curvature has an important role in the performance of such systems. The profiles of the dimensionless radius of curvature along the length of the heat pipe (R^* vs. X^*) for different values of heat input and heat pipe geometry are presented in Fig. 3. In the figure, the value of the radius of curvature at the cold end (R_0) is used as the non-dimensionalizing parameter and is equal to 115.4 μm (triangular) and 200 μm (rectangular).

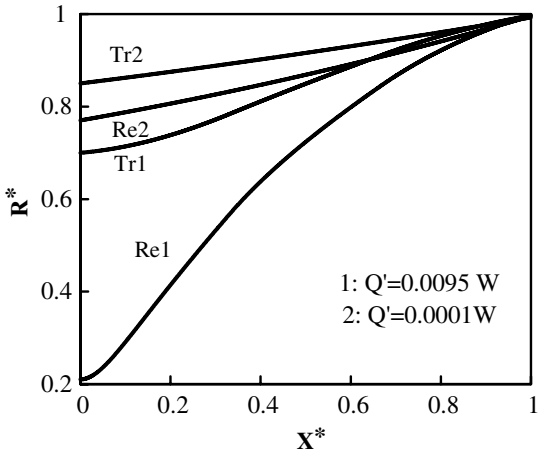

Fig. 3. Variation of dimensionless radius of curvature, R^*, with dimensionless position, X^*, with different values of heat input.

Fig. 3 clearly shows the gradual decrease in R^* as the hot end is approached signifying higher curvature at the hot end. R^* at any location also decreases with increase in heat input (curves Tr2 or Re2 with respect to Tr1 and Re1 respectively). For the same heat input, the liquid meniscus will be more depressed (higher curvature) at the hot end for the case of a rectangular heat pipe compared to a triangular heat pipe. This is a direct result of the apex angle of the corners of the heat pipe and will be discussed in the next subsection. The behavior of the radius of curvature gives a qualitative idea of the capillary pumping. The value of R^* at the hot end or the gradient of R^* can also predict the operating limit of a heat pipe, i.e., the critical heat input for a system controlled by capillary pumping. The critical heat input for such a system, where the flow is sustained by capillary pumping, is defined as the heat input where the flow resulting from the curvature change will not be able to meet the flow requirement due to higher rates of evaporation. For such a case, the radius of curvature of the liquid meniscus at the hot end reaches a value very close to zero and the device approaches its operating limit. From the Young–Laplace equation, it is clear that for the device to operate properly (no generation of dry spot) the radius of curvature should decrease monotonically from the cold to the hot end (dR^*/dX^* should be always positive according to the coordinate system used herein). For the specific cases considered for this study, the critical heat input for triangular and rectangular heat pipes are found to be 0.0205 W and 0.0105 W, respectively (Table 1) for an inclination of 10°. Thus the model correctly predicts that a triangular heat pipe is more efficient (due to enhanced capillary pumping).

The heat pipe inclination has substantial effect on the performance of a heat pipe. The critical heat inputs, as calculated, vary significantly with inclination (Table 1). It is observed that with increase in inclination, the critical heat input decreases due to the opposing (relative to capillary forces, in this configuration) effect of body force (gravity). Therefore, the capillary limit will be reached earlier for a heat pipe with a higher inclination angle. It can also be observed from Table 2 that the body force normal to the coolant flow is very small compared to the force exerted by the pressure jump at the vapor liquid interface. This suggests that the meniscus is symmetric at all corners, at a fixed axial location, irrespective of the position of the corner (top, bottom or side).

The apex angle of the corners of a heat pipe plays an important role in capillary pumping. The variation of the critical heat input for a 2 cm long heat pipe as a function of apex angle (and thus effectively the number of sides) of a polygon is presented in Table 3. The difference in curvature provides the capillary pumping capacity of a micro heat pipe. To pump the same amount of liquid more dimensionless curvature difference between the hot and the cold ends are required since the curvature at the cold end ($1/R_0$) decreases with increase in the apex angle. Moreover, with increase in the number of sides of a regular polygon (increase in the apex angle), the value of friction factor increases as well. For example, the value of friction factor for triangular geometry is

Table 1
Variation of critical heat input (W) with inclination (°) for triangular and rectangular heat pipe of length 2 cm

Inclination (°)	Critical Heat Input $Q_{critical}$ (W)	
	Triangular (200 μm)	Rectangular (400 × 200 μm)
5	0.022	0.0110
10	0.0205	0.0105
20	0.017	0.0068
40	0.012	0.0041
60	0.009	0.0028
90	0.008	0.0023

Table 3
Variation of the critical heat input with number of sides of a regular polygon (length of the sides = 200 μm, overall length = 2 cm, $\Delta T = 5$ °C)

Number of sides of a regular polygon (side 200 μm)	Apex Angle (°)	Critical Heat Flux (W)
6	120	0.0192
8	135	0.0088
12	150	0.00264
20	162	0.00046

Table 2
Variation of body force (N) normal to flow and force due to pressure jump at the liquid–vapor interface (N) with inclination (°) for triangular (200 μm) and rectangular (400 μm × 200 μm) heat pipes of length 2 cm for corresponding critical heat input (W)

Inclination (°)	Body Force ⊥ to Flow (N)		Force due to Pressure Jump at the Interface (N)	
	Triangular × 10^7	Rectangular × 10^7	Triangular × 10^4	Rectangular × 10^4
5	9.76	11.05	9.03	9.029
10	8.65	9.75	9.03	9.029
20	7.40	9.25	9.03	9.029
40	5.33	6.94	9.03	9.029
60	3.70	4.33	9.03	9.029
90	0.0	0.0	9.03	9.029

13.33 whereas for circular it is 16. The friction factor for any other geometry lies in between these two values (Ayyaswamy et al., 1974). The increase in friction factor will cause a decrease in liquid velocity as well. The combined effect of all these will result in a reduction of the capillary pumping capacity. The capillary pumping capacity, therefore, decreases with increase in the apex angle (number of sides).

The variation of axial velocity of the liquid is presented in Fig. 4. The calculated value of the axial velocity from the simultaneous solution of the governing equations is negative due to the coordinate system used herein (origin at the hot end). However, in the subsequent discussion, only the magnitude of the velocity is considered. The absolute value of the axial velocity is zero at the hot end and increases in the evaporative region. This is due to the cumulative effect of replenishing the amount evaporated throughout the evaporator region. In the adiabatic region, although there is no evaporation and condensation, the liquid velocity decreases slightly. This is consistent with the slight increase in the radius of curvature in the adiabatic section (and hence an increase in the liquid flow area). In the condenser region, there is further fall of liquid velocity because condensation results in a sharper increase in the value of radius of curvature. It can also be observed from the figure that with increase in heat input, evaporation increases and to replenish the enhanced amount of evaporated liquid, the velocity increases at a fixed location. It should also be noted that even with an increase in the number of corners for the case of rectangular heat pipe, the liquid flow area is still smaller than that of a triangular one, as predicted by the radius of curvature profile (Fig. 3). This is a result of less capillary suction available at higher values of the apex angle for the rectangular geometry.

To sustain evaporation, liquid should flow from the cold end to the hot end. This requires the liquid pressure

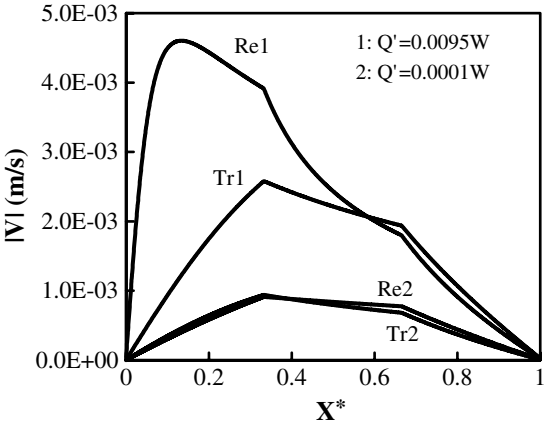

Fig. 4. Variation of the magnitude of axial liquid velocity, $|V|$ (m/s), with dimensionless position, X^*, with different values of heat input.

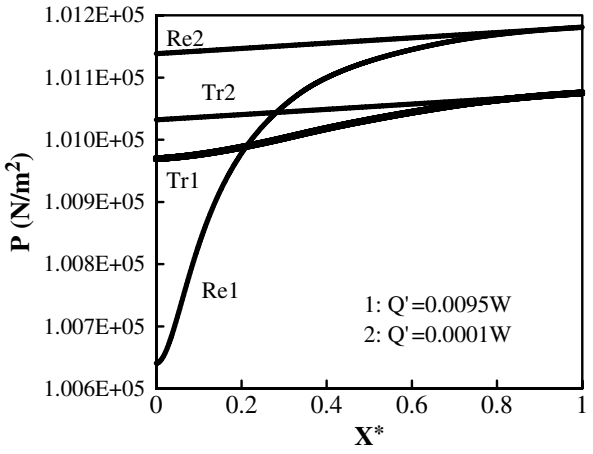

Fig. 5. Variation of liquid pressure, P (N/m^2), with dimensionless position, X^*, with different values of heat input.

should decrease from the cold end to the hot end (dP^*/dX^* is positive for coordinate system used herein). The variation of liquid pressure with position is presented in Fig. 5. The overall liquid pressure drop across the whole length of the heat pipe can be expressed as (integrating Eq. (1))

$$\Delta P = \frac{\sigma}{R_0}\left[\frac{1}{R^*_{\text{hot end}}} - 1\right] \tag{9}$$

where R_0 is the radius of curvature at the cold end and is a constant for a particular geometry. The dimensionless radius of curvature at the hot end $R^*_{\text{hot end}}$ decreases with increase in heat input. Hence, the overall pressure drop increases with increase in heat input. The difference in the values of $R^*_{\text{hot end}}$ between the triangular and the rectangular cases for the same heat input is appreciable. For example, for a heat input of 0.0095 W the value of $R^*_{\text{hot end}}$ for the triangular heat pipe is 0.70, and that for the rectangular it is 0.21 (refer Fig. 3). On the other hand, R_0 will be 115.4 μm and 200 μm for the triangular and the rectangular cases, respectively. Thus for the two geometries considered herein, the pressure drop in the rectangular heat pipe will be substantially more than the triangular one for a heat input of 0.0095 W. Therefore, under the present conditions and geometries, the triangular heat pipe performance is better than rectangular one.

The theoretical development presented herein can effectively be used to predict the onset and propagation of the dry-out length for a set of process variables. At the critical heat input, the radius of curvature at the hot end becomes very close to zero. Any higher value of heat input will propagate the dry region towards the cold end, as capillary pumping will not be able to sustain the increased rate of evaporation. The dry length of the heat pipe is known as dry-out length. The location of the dry-out point can be estimated numerically by changing the initial value of integration (from $X^* = 0.0$

to a finite value of X^* where R^* is close to zero), so as to meet the boundary conditions at the cold end i.e., $R^* = 1.0$ within a tolerance limit. The X^* value (where $R^* \rightarrow 0.0$) thus obtained, denotes the non-dimensional dry-out length of the heat pipe corresponding to the particular set of process variables. Using this methodology, the dry-out length for both heat pipes is evaluated as a function of heat input and is presented in Fig. 6. As can be seen from the figure, the dry-out length increases with increase in heat input for particular heat pipe geometry and for an inclination of 10°. Due to the enhanced capillary suction present in a triangular heat pipe, the dry out length is smaller compared to that of a rectangular heat pipe for a set of process variables. Thus, the methodology developed herein can be effectively used to predict not only the formation of the dry region but a quantitative estimation of its propagation as well.

In the study by Anand et al. (2002), experiments were carried out in a specially designed cell to study the onset and propagation of dry out point on a micro grooved silicon surface with pentane as the coolant liquid. Chemical machining method was used to fabricate V-shaped axial micro grooves on a silicon substrate. Controlled heat was supplied to the top of the substrate and axial temperature distribution was accurately measured as a function of input heat and inclination of the substrate to the horizontal. The comparison between the dry (without liquid) and wet (with liquid) temperature profiles was used to locate the dry-out point and its propagation as a function of inclination angle and supplied heat flux. 33 V-grooves of 2 cm length and 100 μm wide with groove depth of 68.82 μm were used together with a groove pitch of 200 μm. Pentane was used as the coolant. A resistance heater was used as the source of heat and the backside of which was carefully insulated to ensure that all of the supplied heat into the system. Careful design of the system excluded the possibility of any vapor loss from the system. A series of small thermocouples accurately measured the temperature profiles as functions of heat input to the system and inclination angle. These two parameters (heat input and angle were varied carefully so that a portion of the grooved plate becomes dry and the propagation of the dry out point along the length of the channel were evaluated from a comparison of the temperature profiles. It was postulated that since there was no vapor loss from the system and the same amount of input power was used in both the wet and dry (no coolant used) runs, the two temperature profiles would be almost identical for the region near the heater from which the liquid had completely receded (dry out) as a result of increase in inclination angle (opposing body force). As the inclination angle and hence the opposing body force was increased keeping the power input and amount of liquid constant, the top portion (near the heater) of the two profiles nearly overlapped (up to the third thermocouple), emphasizing that dry out condition has been reached in that region (Fig. 7). A further increase in inclination resulted in further propagation of the dry out region, away from the heater towards the bulk liquid pool. A series of such runs at different power inputs generated a data set of dry out point locations as function of power inputs and angles of inclination.

The axial distribution of the heat used for evaporation is determined in numerous small sections of the substrate using the experimentally obtained temperature profile. From the experimentally measured temperature profile, the convective heat transfer coefficients of all the four sides of the substrate and the corresponding convective heat losses are evaluated as functions of position. The conduction heat rate in the solid is also evaluated from the known temperature profile. The substrate is divided into 50 small sections each with a length equal to

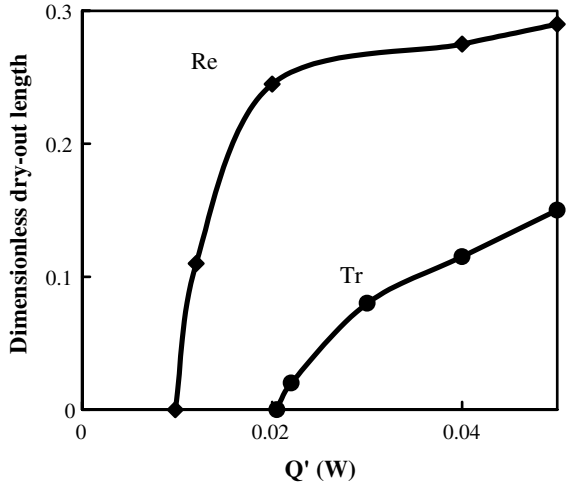

Fig. 6. Variation of the dimensionless dry-out length.

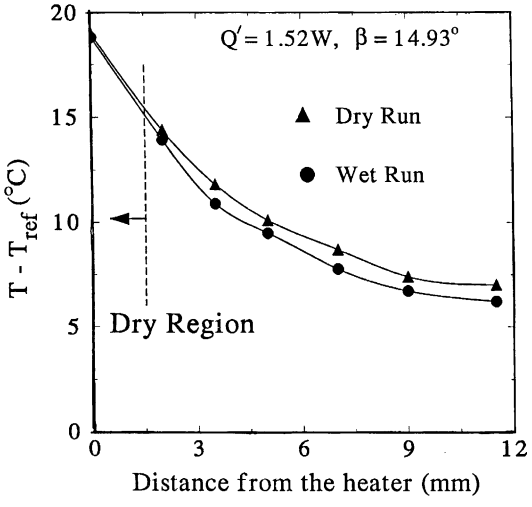

Fig. 7. Temperature profile and dry-out length for a fixed power input and inclination (Anand et al., 2002).

Table 4
Comparison between the experimental (Anand et al., 2002) and theoretical dry-out length (in mm)

Power (W)	Inclination (°)	Calculated dry-out length, mm	Experimental dry-out length Anand et al. (2002), mm	T_{amb} (°C)
1.52	14.93	6.4	6.5	32.6
1.52	21.64	7.1	7.5	35.0
1.52	26.56	10.0	10.00	35.0
1.52	38.66	12.3	12.5	33.0
1.52	43.16	13.9	14.2	35.0
1.71	38.66	15.7	16.5	32.6
1.71	90.00	15.9	16.5	32.6

4×10^{-4}m. For each section, from the known value of the heat entering, the convective losses and the heat leaving by conduction are subtracted to obtain the evaporative heat flux from that section. The evaporative heat flux distribution thus obtained is used subsequently to solve the model equations (in Eqs. (5) and (6)) for a V-groove geometry.

The comparison of calculated and experimental dry-out length is presented in Table 4. It may be observed from the table that the model predicted values of dry out length are in very good agreement with the experimental data. For a heat input of 1.52 W and an inclination of 14.93°, the experimental and model predicted values are 6.5 and 6.4 mm respectively. The model also correctly predicts, both qualitatively as well as quantitatively the increase in the dry region as the inclination angle is progressively increased to 43.16°. Thus the relatively simple generalized model, based on first principles, proposed in this study, correctly predicts the behavior of micro grooved heat pipes in terms of trends in radius of curvature, axial liquid velocity and pressure and through a satisfactory agreement with the experimental results of a previous study.

4. Conclusions

A simple generalized model of heat transfer in a heat pipe of any geometrical shape is developed utilizing a macroscopic approach. Two different heat pipes namely, rectangular and triangular are considered for case study. It is found that the effects of body forces are small compared to the pressure jump force at the liquid vapor interface force and thus, the liquid will be equally distributed among all corners at any location. An increase in the apex angle reduces the capillary suction capability and thus the transport capacity of a triangular heat pipe is more than that of a rectangular one. The profile of the radius of curvature is used to predict the onset of the dry-out point. The dry-out length increases with increase in heat input and inclination. The enhanced capillary pumping capacity of the triangular heat pipe compared to a rectangular heat pipe is manifested by a smaller value of the dry-out length for the same heat input. The model is validated with the experimental results available in literature. The present study can be extended to study the effect of wettability and viscosity on the performance of heat pipe and to design of the heat pipe.

Acknowledgments

This work is partially supported by a grant from the Board of Research in Nuclear Sciences (BRNS), Government of India under the sanction number 2001/36/12/BRNS/726. Any opinions, findings and conclusions or recommendations expressed in this paper are those of the authors and do not necessarily reflect the views of the BRNS.

Appendix A. For polygonal heat pipe with equal sides

$$R_0 = \frac{a \sin \alpha}{2 \cos(\alpha + \gamma)}$$

where a is side length of the polygon or smaller side of rectangle

$$Q = 3Q'/naL$$

where Q' is the heat input per channel and Q is the heat flux.

$$\alpha = (n-2)\pi/2n$$

where α is half apex angle and n is the number of sides of the polygon

$$W_b = na$$

where W_b is groove pitch.

A.1. For the rectangular heat pipe (side ratio 1:2)

$$R_0 = \frac{a \sin \alpha}{2 \cos(\alpha + \gamma)}$$

$$Q = 3Q'/2(a + a_1)L$$

where a_1 is the larger side of rectangle.

$$\alpha = \pi/4$$

$$W_b = 2(a + a_1)$$

A.2. For the triangular (equilateral) heat pipe

$$n = 3$$

$$R_0 = \frac{a \sin \alpha}{2 \cos(\alpha + \gamma)}$$

$$W_b = na$$

$$Q = 3Q'/(W_b L)$$

$\alpha = \pi/6$

Geometry of one corner of the polygonal heat pipe is presented in Fig. A.1.

The shaded area in Fig. A.1 is the cross-sectional area of the liquid in the heat pipe. The cross-section area of one corner is expressed as

$$A_1' = \text{Area of ACBD} + \text{Area of } \Delta ABC - (\text{Area of sector AOB} - \text{area of } \Delta AOB)$$

The line diagram of section OBC in Fig. A.1 is presented in Fig. A.2 in detail.

From Fig. A.2, AC and BC are the tangents to the liquid meniscus.

$\angle CAD = \gamma$
$\angle ADC = \alpha$
$\angle ACB = 2(\alpha + \gamma)$
$\angle AOB = \phi = \pi - 2(\alpha + \gamma)$
$R_0 = \frac{a \sin\alpha}{2\cos(\alpha+\gamma)}$

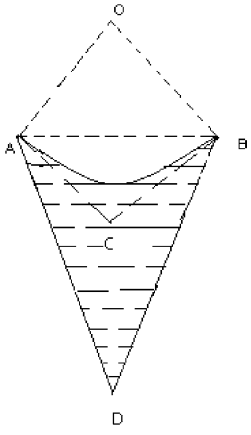

Fig. A.1. Geometry of a liquid filled corner.

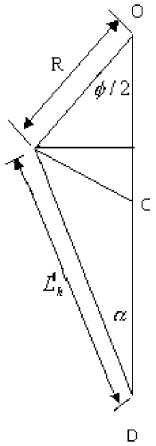

Fig. A.2.

$L_h' = R\frac{\cos(\alpha+\gamma)}{\sin\alpha}$
$L_h = nL_h'$
$R_1 = nR\phi$
Area of ACBD $= \frac{R^2\cot(\alpha+\gamma)\cos(\alpha+\gamma)\sin\gamma}{\sin\alpha}$
Area of $\triangle ABC = R^2\cot(\alpha+\gamma)\cos^2(\alpha+\gamma)$
Area of sector AOB $= \phi R^2/2$
Area of $\triangle AOB = R^2\cos(\alpha+\gamma)\sin(\alpha+\gamma)$

Hence

$$A_1' = R^2\left[\{\cot(\alpha+\gamma) - \varphi/2\} + \frac{\cot(\alpha+\gamma)\cos(\alpha+\gamma)\sin\gamma}{\sin\alpha}\right]$$

and

$$A_1 = nA_1' = nR^2\left[\{\cot(\alpha+\gamma) - \varphi/2\} + \frac{\cot(\alpha+\gamma)\cos(\alpha+\gamma)\sin\gamma}{\sin\alpha}\right] = B_1R^2$$

where

$$B_1 = n\left[\{\cot(\alpha+\gamma) - \varphi/2\} + \frac{\cot(\alpha+\gamma)\cos(\alpha+\gamma)\sin\gamma}{\sin\alpha}\right]$$

$$B_2 = \frac{\mu K'\cos^2(\alpha+\gamma)}{2\sin^2\alpha\left[\frac{\cot(\alpha+\gamma)\cos(\alpha+\gamma)\sin\gamma}{\sin\alpha} + \{\cot(\alpha+\gamma) - \varphi/2\}\right]^2}$$

References

Anand, S., De, S., DasGupta, S., 2002. Experimental and theoretical study of axial dry-out point for evaporative from V-shaped microgrooves. Int. J. Heat Mass Transfer 45, 1535–1543.

Anderson, D.M., Davis, S.H., 1995. The spreading of volatile liquid droplets on heated surfaces. Phys. Fluids 7, 248–265.

Ayyaswamy, P.S., Catton, I., Edwards, D.K., 1974. Capillary Flow in triangular grooves. ASME J. Appl. Mech. 41, 332–336.

Babin, B.R., Peterson, G.P., Wu, D., 1990. Steady state modeling and testing of a micro heat pipe. J. Heat Transfer 112, 595–601.

Bankoff, S.G., 1990. Dynamics and stability of thin heated liquid films. J. Heat Transfer 112, 538–546.

Catton, I., Stroes, G.R., 2002. A semi-analytical model to predict the capillary limit of heated inclined triangular capillary grooves. J. Heat Transfer 124 (1), 162–168.

Cotter, T.P., 1984. Principles and prospects of micro heat pipes. In: Proceedings of the Fifth Int. Heat Pipe Conference, Tsukuba, Japan, pp. 328–332.

DasGupta, S., Schonberg, J.A., Kim, I.Y., Wayner, P.C., 1993a. Use of augmented Yong-Laplace equation to model equilibrium and evaporation extended meni-sci. J. Colloid Interface Sci. 157, 332–342.

DasGupta, S., Schonberg, J.A., Wayner, P.C., 1993b. Investigation of an evaporative extended meniscus based on the augmented Yong-Laplace equation. J. Heat Transfer 115, 201–208.

DasGupta, S., Plawsky, J.L., Wayner, P.C., 1995. Interfacial force field characterization in a constrained vapor bubble thermosyphon. AIChE Jr. 41, 2140–2149.

Derjaguin, B.V., Chyraev, N.V., 1976. The definition of disjoining pressure and its importance in the equilibrium and flow of thin films. Colloid J. USSR 38, 438–448.

Gee, M.L., Hearly, T.W., White, L.R., 1989. Ellipsometric studies of alkenes adsorption on quartz. J. Colloid Interface Sci. 131 (1), 18–23.

Gokhale, S., Plawsky, J.L., Wayner Jr., P.C., DasGupta, S., 2004. Experimental measurement of pressure gradient and fluid flow in a small spreading drop during condensation. Physics of Fluids 16 (6), 1942–1955.

Ha, J.M., Peterson, G.P., 1998. Analytic prediction of axial dry-out point for evaporating liquids in axial microgrooves. J. Heat Transfer 120, 452–457.

Khrustalev, D., Faghri, A., 1994. Thermal analysis of a micro heat pipe. J. Heat Transfer 116 (1), 189–198.

Khrustalev, D., Faghri, A., 1995. Thermal characteristics of conventional and flat miniature axially grooved heat pipes. J. Heat Transfer 117, 1048–1054.

Ma, H.B., Peterson, G.P., 1996. Experimental investigation of the maximum heat transport in triangular grooves. J. Heat Transfer 118, 740–746.

Md. Khan, A.A., Mishro, S., De, S., DasGupta, S., 1999. An experimental and theoretical investigation of evaporative cooling from V-shaped microgrooves. Intl. J. Transport Phenom. 1, 277–289.

Moosman, S., Homsy, S.M., 1980. Evaporating menisci of wetting fluids. J. Colloid Interface Sci. 73, 212–223.

Peterson, G.P., Ma, H.B., 1996. Theoretical analysis of the maximum heat transport in triangular grooves: a study of idealized micro heat pipe. J. Heat Transfer 118, 731–739.

Ravikumar, M., DasGupta, S., 1997. Modeling of evaporation from V-shaped microgrooves. Chem. Eng. Comm. 160, 225–248.

Renk, F., Wayner, P.C., 1979. An evaporating ethanol meniscus; Part II: analytical studies. J. Heat Transfer 101, 55–62.

Stephan, P.C., Busse, C.A., 1992. Analysis of heat transfer coefficient of grooved heat pipe evaporator walls. Int. J. Heat Mass Transfer 35, 383–391.

Swanson, L.W., Herdt, G.C., 1992. Model of the evaporative meniscus in a capillary tube. J. Heat Transfer 114, 434–441.

Swanson, L.W., Peterson, G.P., 1995. The interfacial thermodynamics of micro heat pipes. J. Heat Transfer 115, 195–201.

Troung, J.G., Wayner, P.C., 1987. Effects of capillary and Vander Waals dispersion forces on the equilibrium profile of a wetting liquid: theory and experimental. J. Chem. Phys. 87, 4180–4188.

Wayner Jr., P.C., 1991. The effect of interfacial mass transport on flow in thin liquid films. Colloids Surfaces 52, 71–84.

Wayner Jr., P.C., Kao, Y.K., LaCroix, L.V., 1976. The interline heat transfer coefficient of an evaporative wetting film. Int. J. Heat Mass Transfer 19, 487–492.

Wu, D., Peterson, G.P., 1991. Investigation of the transient characteristics of a micro heat pipe. J. Thermophys. 5, 129–134.

Xu, X., Carey, V.P., 1990. Evaporative from microgrooved surface—an approximate heat transfer model and its comparison with experimental data. J. Thermophys. 4, 512–520.

Zheng, L., Plawsky, J.L., Wayner Jr., P.C., DasGupta, S., 2004. Stability and oscillations in an evaporating corner meniscus. J. Heat Transfer 126, 169–178.